Journal of Materials Chemistry A

Accepted Manuscript

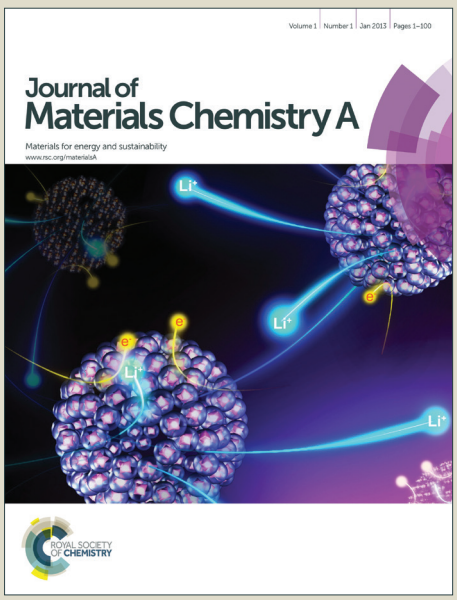

ROYAL SOCIETY OF CHEMISTRY

www.rsc.org/materialsA

Journal Name

ARTICLE

Proton conducting $H_5BW_{12}O_{40}$ electrolyte for solid supercapacitors

Han Gao, Alvin Virya and Keryn Lian*[a]

Received 00th January 20xx,
Accepted 00th January 20xx

DOI: 10.1039/x0xx00000x

www.rsc.org/

$H_5BW_{12}O_{40}$ (BWA), a heteropolyacid with B^{3+} as the central heteroatom, was developed as an electrolyte for solid supercapacitors. Structural properties of synthesized BWA were investigated using FTIR and XRD and were compared to a known silicotungstic acid ($H_4SiW_{12}O_{40}$, SiWA) electrolyte. Factors affecting the cell voltage of supercapacitors using liquid BWA and SiWA electrolytes were identified using an in-situ electrode potential tracking method. The respective contributions of electrodes and electrolyte were revealed and BWA showed a wider potential window than SiWA. Solid supercapacitors enabled by BWA- and SiWA-based polymer electrolytes were demonstrated and exhibited excellent rate performance. The solid device leveraging a BWA-based polymer electrolyte achieved a cell voltage of 1.6 V, better than the 1.4 V achieved by the SiWA-based device.

Introduction

Proton-conducting polymer electrolytes have shown great promise and become key enablers for solid-state, light weight, and flexible supercapacitors.[1] Most of these electrolytes are based on perfluorosulphonic acid membranes (e.g. Nafion® and derivatives)[1-4] or polymer gel electrolytes with liquid acids (e.g.H_3PO_4 or H_2SO_4) blended into the polymer hosts, such as polyvinyl alcohol (PVA).[1, 5-7] Their performance is strongly dependent on the humidity and the temperature of the operating environment. For solid-state supercapacitors, polymer electrolytes are required to have high ionic conductivity and good environmental stability at ambient conditions. Solid proton conductors in a polymer-in-salt configuration have proven to be a good alternative.[1, 8, 9]

The most promising solid proton conductors are Keggin-type heteropolyacids (HPAs). These are hydrous acids which possess the highest proton conductivity at room temperature among inorganic solid proton conductors.[10-14] HPAs belong to a large family of metal-oxygen clusters of early transition metals formulated as $H_z[X_xM_mO_y]$, where M is the addenda atom and X is the heteroatom.[14-16] Two familiar HPAs are silicotungstic acid (SiWA, $H_4SiW_{12}O_{40}$) and phosphotungstic acid (PWA, $H_3PW_{12}O_{40}$). Both share the same Keggin structure (i.e. x=1, m=12, y=40). Aqueous HPA solutions[17-20] and solid HPAs[21-23] have been demonstrated as electrolytes for fuel cells and supercapacitors. However their electrochemical stability potential window is limited due to the electrochemically active nature of the heteropolyanions.[15, 16] A narrow potential window is a shortcoming of almost all aqueous-based electrolytes. For HPAs, the electrochemical stability window can be fine-tuned by choosing constituent addenda and heteroatoms, since the potential of their redox peaks is highly dependent on the composition of their primary Keggin anions.[15, 16, 24] The reduction potentials for Keggin anions decrease linearly with the charge they carry. These changes in redox potentials lead to a variation of cell voltage when used as electrolyte.

In previous studies, we have developed a SiWA-based polymer electrolyte system and demonstrated it in ultra-high rate supercapacitor applications.[8, 25] The polymer electrolyte-enabled thin and flexible solid electrochemical double layer capacitor (EDLC) exhibited an excellent high rate capability of 50 Vs^{-1} in cyclic voltammograms (CV) and a 10 ms time constant in impedance analyses at room temperature,[8] the highest rate ever reported. However, the voltage window of the SiWA-PVA system was limited and needs to be further expanded.

In the current study, Keggin-type $H_5BW_{12}O_{40}$ (henceforth referred to as BWA) where B^{3+} is the central heteroatom was investigated and compared to SiWA (Si^{4+} as central heteroatom). Our goal was to first expand the electrochemical stability window of the solid HPA while maintaining its high proton conductivity, and then to integrate it into polymer electrolytes for solid-state supercapacitors. Concurrently, a systematic study of the structure and properties of BWA- and SiWA-based aqueous electrolytes was performed and their influence on the maximum cell voltage was investigated. Carbon nanotube-graphite (referred as CNT-graphite) electrodes were utilized for electrochemical double layer capacitors (EDLCs) in both liquid and solid-state electrolytes.

[a] Department of Materials Science and Engineering, University of Toronto, Toronto, Ontario, Canada M5S 3E4.
* E-mail: keryn.lian@utoronto.ca; Tel: +1-416-978-8631

Experimental

Preparation of heteropolyacids

$H_4SiW_{12}O_{40}\cdot xH_2O$ (SiWA) was used as-received from Alfa Aesar. $H_5BW_{12}O_{40}\cdot xH_2O$ (BWA) was synthesized by a modified Copaux's method.[26] Briefly, $Na_2WO_4\cdot 2H_2O$ (5 g) was mixed with H_3BO_3 (4 g) in hot water (25 mL). The solution was adjusted to pH 5.5 using 6N HCl and heated at 60 °C for 2 hours under stirring. Subsequently, the pH was further adjusted to 3.8 using 6N HCl and the solution was heated at 80 °C for 6 hours. Finally, the solution was allowed to cool to room temperature and to set for 6 hours. Solid precipitates were filtered out and the filtrate solution was extracted with diethyl ether. The isolated solid was washed with DI H_2O and dried, yielding ca. 2 g of a white crystal product.

Preparation of polymer electrolytes

SiWA- and BWA-based solid polymer electrolytes were prepared by mixing a 5 wt.% PVA (Alfa Aesar, MW=145000 $gmol^{-1}$) aqueous solution with SiWA or BWA to form a precursor solution. Glutaraldehyde ($CH_2(CH_2CHO)_2$, Alfa Aesar) was added as a polymer cross-linking agent. The glutaraldehyde to PVA unit molar ratio was controlled at 0.013 as reported earlier.[8] Glycerol was added to the electrolyte as a plasticizer. The electrolyte films had a composition of ca. 80 wt% SiWA or BWA, 10 wt% glycerol, and 10 wt% cross-linked PVA, assuming that most of the free water was removed during the film drying process. The films had a thickness of ca. 150 µm.

Material characterizations

Infrared (IR) spectra were recorded on a Thermo Scientific Nicolet iS5 FT-IR spectrometer with iD1 transmission module at room temperature. A few drops of the HPA solution was applied on the central portion of an IR transparent silicon window. Water was allowed to evaporate under ambient conditions to form solid acids.

X-ray diffraction (XRD) measurements were carried out using a Philips XRD system, including a PW 1830 HT generator, a PW 1050 goniometer, and PW 3710 control electronics. The samples were analyzed with a Cu-Kα source operating at 40 kV/40 mA. The diffraction patterns were recorded from 5° to 50° 2θ with a step scan of 0.02° 2θ and a scan step time of 2 seconds. All XRD samples were heated at 80-90 °C overnight before being characterized.

Construction of liquid and solid cells

The electrolytes were characterized in either 3- or 2-electrode cell configurations using two types of working electrodes: (1) stainless steel foil as metallic electrodes to characterize the ionic conductivity of the electrolytes; and (2) CNT-graphite on Ti foils as EDLC electrodes.

The procedure of manufacturing CNT-graphite electrodes was described in a previous report.[27] The carbon loading was ca. 3 $mgcm^{-2}$, which contained 22% CNT, 63% graphite, and 15% PVA binder (all in wt. %). The geometric area of the stainless steel and CNT-graphite electrodes was 1 cm^2. Ag/AgCl and Pt mesh were used as reference and counter electrode, respectively, in 3-electrode cells. The open-circuit potential of the CNT-graphite electrodes was ca. 0.3 V (vs. Ag/AgCl) in both 0.05 M SiWA and BWA.

The liquid electrochemical cells were beaker cells, in which two electrodes were connected to a potentiostat. An Ag/AgCl reference electrode was added into the cell and connected externally to a dual-channel digital oscilloscope (DGS-122).[28] In this configuration, the positive and negative electrodes were charged and discharged as a regular capacitor, while the potential variation at each electrode was simultaneously tracked and recorded. This in-situ electrode potential tracking method can characterize an individual electrode at the device level, which is particularly beneficial for analyzing the cell voltage of supercapacitors.

The solid electrochemical cells were assembled in the following steps: (1) Coating polymer electrolyte precursor solutions on both positive and negative electrodes and drying at ambient temperature; (2) sandwiching the two electrodes from step (1) for 20 min under 20 to 30 kPa pressure at ambient temperature; and (3) protecting with tapes.[29] All cells were then stored at 25 °C, 45% relative humidity (RH) in a desiccator overnight to achieve a steady-state condition before conducting electrochemical tests.

Electrochemical characterizations

Cyclic voltammetry (CV) and electrochemical impedance spectroscopy (EIS) were performed using a CHI 760 C bipotentiostat. The EIS spectra were recorded from 100 kHz to 1 Hz (for metallic cells) or 0.01 Hz (for CNT-graphite cells) with a 5 mV amplitude. Areal capacitance was calculated using charge (Q) divided by voltage window (U) and the geometric surface area of the electrode. The conductivity of the electrolytes was calculated using the cell constant (obtained with 1M KCl) and the equivalent series resistance (ESR), which was extracted from the EIS measurements.[27] The reported conductivity was based on an average of at least five cells. All electrochemical tests were conducted at room temperature.

Results and discussion

Confirmation of the Keggin structure

The structure of the synthesized material was characterized and compared to a known HPA (in this case SiWA) to confirm the presence of a stable Keggin anion and, thus, a solid HPA that can release protons. The FTIR spectra of HPAs share similar vibrational features in the 400-1100cm^{-1} region as the characteristic structures of the primary Keggin unit.[30-32] Fig. 1 compares the structure of the synthesized BWA in this frequency region to that of SiWA. Table 1 summarizes the wave numbers of the bands with their associated bonding interactions for the two spectra.

Both IR spectra have similar features, representing typical Keggin structures. In the 400-1100 cm^{-1} region, structure and interaction of the HPA are well characterized as vibrational stretching modes of four types of oxygen: tetrahedral oxygen (O_a) with a center heteroatom, edge sharing oxygen (O_b), corner sharing oxygen (O_c), and terminal oxygen (O_d).[33-37] The tetrahedral oxygen (O_a) connects the central heteroatom X (i.e.

Table 1 FTIR band positions and associated bonding information for SiWA and BWA.

Wavenumber		Band assignment
SiWA	BWA	
1019[a]	1002[a]	N/A
1018[b]	1006[c]	
1018[c]	1010[d]	
980[a]	961[a]	$W=O_d$ stretching
982[b]	960[c]	
980[c]	960[d]	
925[a]	912[a]	$X-O_a$ stretching
930[b]	914[c]	(X=Si, B)
926[c]	920[d]	
880[a]	902[d]	$W-O_b-W$
885[b]		stretching
878[c]		
778[a]	814[a]	$W-O_c-W$
792[b]	810[c]	stretching
779[c]	820[d]	

[a] present study; [b] reference [33]; [c] reference [34]; [d] reference [35]

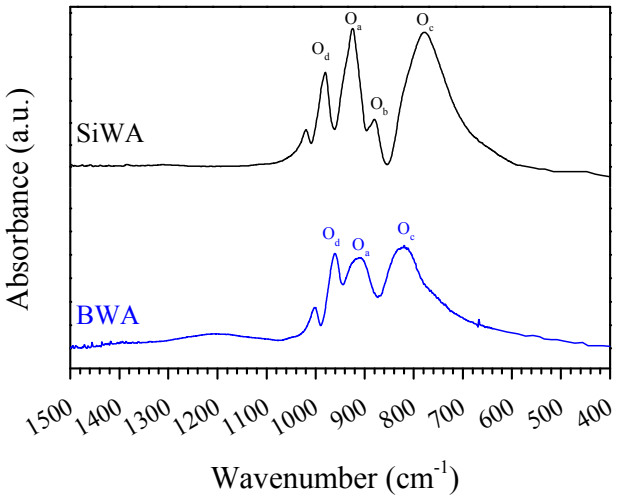

Figure 1: FTIR spectra of commercial SiWA as well as synthesized BWA on IR transparent Si windows.

Si or B) to a W atom. The two types of sharing oxygen atoms (O_b and O_c) bridge two W atoms in the neighboring octahedral, whereas the terminal oxygen atom (O_d) is bonded to only one W atom. Although the interaction of $W-O_b-W$ was not observed in the IR spectrum of BWA, similar to the study by Hu et al.,[34] Fig. 1 still confirmed the successful synthesis of the Keggin anion structure.

The composition and structure of the bulk BWA crystals was investigates with XRD. Since the structure of a solid HPA is highly dependent on the amount of co-crystallized water in the crystal lattice, their XRD patterns vary significantly with the levels of hydration.[12, 38-40] To compare BWA and SiWA at the same level of hydration, both samples were heated at 80-90 °C overnight before characterization. Fig. 2 depicts the XRD patterns of BWA and SiWA. The narrow peaks in the XRD patterns imply a long-range order crystal structure. Both BWA and SiWA patterns were very similar and indicative of the same characteristic crystal structure. Experimental evidence verified the high purity of the synthesized BWA.

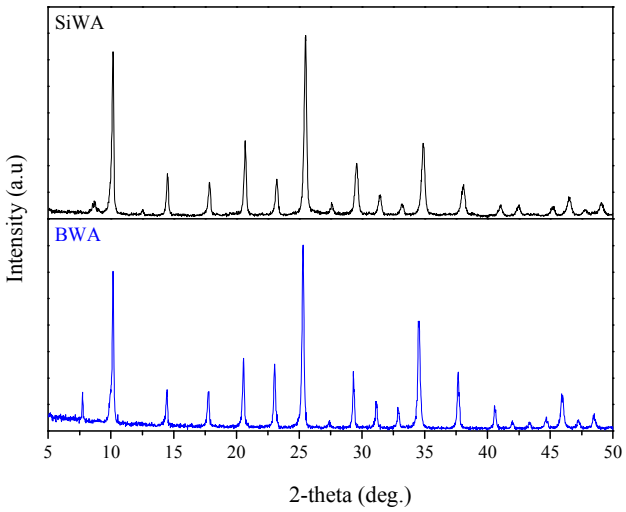

Figure 2: Powder XRD patterns of commercial SiWA as well as synthesized BWA, after 2-day heating at 80-90 °C.

Ionic conductivity

A test vehicle using two stainless steel electrodes was employed to measure the ionic conductivity of aqueous solutions of synthesized BWA. As a baseline, H_2SO_4 and SiWA with the same concentrations were included in the comparison. Fig. 3a shows the ionic conductivity of SiWA, BWA, and H_2SO_4 at three concentrations. As expected, ionic conductivity increased with an increase in concentration. BWA showed the highest ionic conductivity while H_2SO_4 had the lowest conductivity across the tested concentration range.

To understand the origin of the high ionic conductivity of the BWA electrolyte, the molar ionic conductivity of the three solutions was plotted in Fig. 3b. Since all three solutions are strong electrolytes, Kohlrausch's law was used to estimate the limiting molar ionic conductivity for each electrolyte. Both BWA and SiWA exhibited higher molar ionic conductivity than H_2SO_4, resulting from their higher ionic strength and anion mobility. It has been reported that the mono-valent anion of SiWA ¼$[SiW_{12}O_{40}]^-$ demonstrates a high limiting molar conductivity of 237 Scm^2mol^{-1},[41] much higher than that of

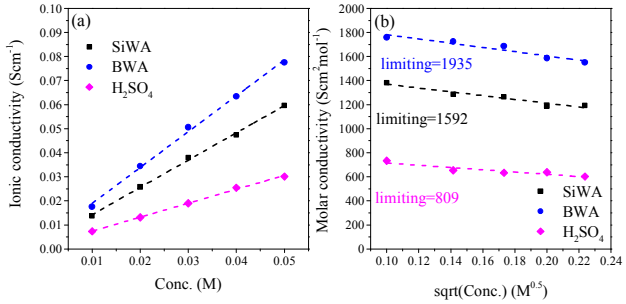

Figure 3: Comparison of SiWA, BWA, and H_2SO_4 in terms of (a) ionic conductivity in 0.01, 0.02, 0.03, 0.04, and 0.05 M concentrations; and (b) molar conductivity as a function of concentration.

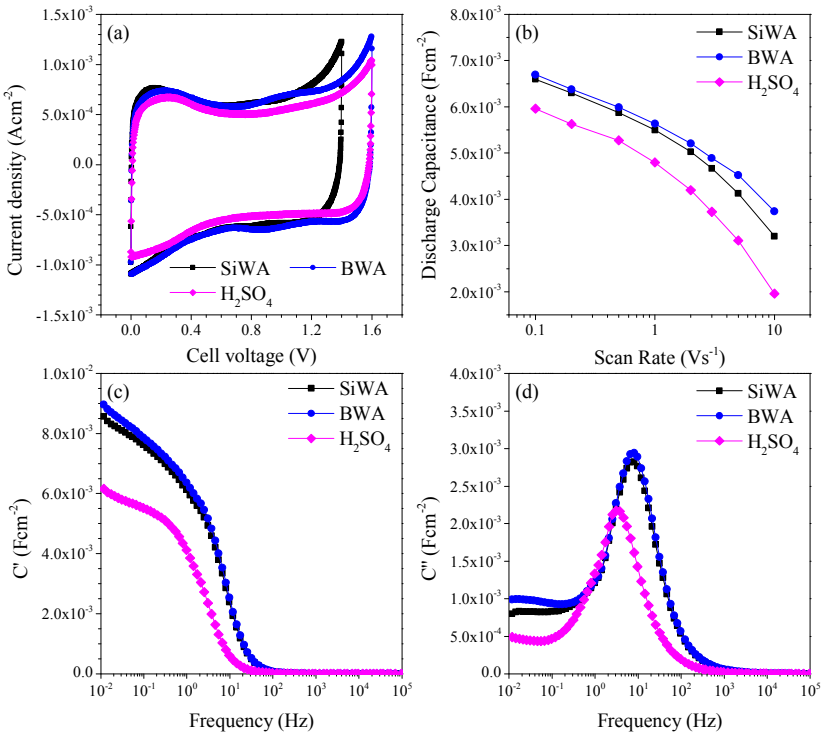

Figure 4: (a) CVs of EDLC cells with 2 CNT-graphite electrodes in 0.05 M aqueous SiWA, BWA, and H_2SO_4; (b) capacitance variation at different scan rates; (c) real part of ac capacitance (C'); and (d) imaginary part of ac capacitance (C").

½$[SO_4]^-$ (80 Scm^{2}mol^{-1})[42] due to the un-solvated nature of SiWA anion. For the same reason, BWA was expected to exhibit similar anion mobility. Because of the high mobility together with a greater amount of dissociated protons, both HPAs demonstrated higher limiting molar conductivity than H_2SO_4. BWA showed even higher limiting molar conductivity (343 Scm^{2}mol^{-1}) than SiWA, due to its extra protons.[42]

Electrochemical characterization of carbon EDLC

Having confirmed the structure of BWA and demonstrated its high ionic conductivity, BWA was studied as an electrolyte for liquid EDLC devices and compared to an EDLC using a SiWA electrolyte. The CVs of both BWA- and SiWA-based EDLCs were overlaid on that of a H_2SO_4-based EDLC (Fig. 4a). The BWA-based EDLC achieved a voltage window of 1.6 V, comparable to that of H_2SO_4, while the SiWA-based EDLC reached only 1.4 V. This difference in cell voltage will be discussed in the next section. The capacitance of the three EDLCs at different scan rates is shown in Fig. 4b. Similar to the trend in conductivity, the capacitance increased with the increase in scan rate in the order H_2SO_4<SiWA<BWA. Since the charge separation process in EDLCs is dominated by the rate of ionic movement and the number of dissociated ions in the electrolyte, as expected BWA showed the highest capacitance.

EIS analysis was performed to complement the dc characterization and to confirm the trend in Fig. 3 and Fig. 4b. We used the approach of Taberna et al.[43] to separate the real part of the capacitance (C') from its imaginary part (C") and plot them as a function of frequency (Figs. 4c and d). C' represents the accessible capacitance per area of the device at the corresponding frequency, while C" is related to the energy dissipation of an irreversible process. The maximum of the C" vs. frequency curve represents a time constant at which a transition from resistive to capacitive behavior occurs. At the low frequency portion of Fig. 4c, both SiWA and BWA cells approached 9 mFcm^{-2} while C' of the H_2SO_4 cell approached 6 mFcm^{-2}, consistent with the values obtained from CV profiles (Fig. 4a) and the trend in capacitance (Fig.4b). C" of the H_2SO_4 cell and the HPA-enabled ELDCs exhibited maxima at around 2 Hz and 8-10 Hz, respectively (Fig. 4d). This characteristic relaxation frequency analogous to the RC time constant of a supercapacitor.[43] Even though the BWA-enabled cell showed the highest capacitance, it exhibited the smallest time constant (i.e. higher relaxation frequency). This is another indication of good conductivity, making BWA an ideal electrolyte for supercapacitors.

Analysis of operating cell voltage

The wider electrochemical operation window of BWA-enabled EDLCs is interesting and is the subject of further investigation. Before analyzing the capacitor cell voltage, CVs of a single CNT-graphite electrode in 0.05 M SiWA and 0.05 M BWA were first acquired, and are depicted in Fig. 5. It is clear from the CVs that both HPAs are redox active at negative potentials. The positive potential limit for SiWA was about 1.2 V due to oxygen evolution while the negative potential limit was ca. -0.25 V, corresponding to the redox reactions of its anion,[44, 45] yielding a 1.45 V potential window for SiWA with the CNT-graphite electrode. In the CV of SiWA we can observe a pair of redox peaks from the carbon functional groups at around 0.3-0.4 V,

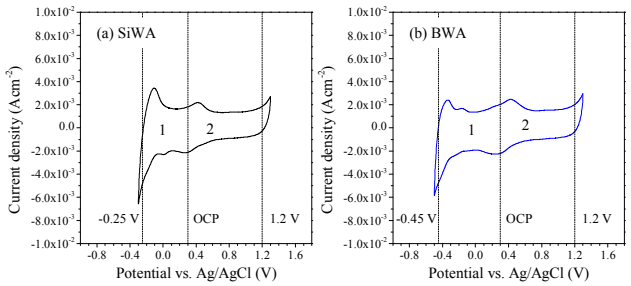

Figure 5: CVs of a CNT-graphite electrode in 0.05 M aqueous (a) SiWA and (b) BWA (scan rate = 100 mVs^{-1}).

which are often seen in other aqueous electrolytes such as H_2SO_4. The CV of BWA (Fig. 5b) with the same electrode material had a negative potential limit of ca. -0.45 V and a positive limit of 1.2 V, yielding a 1.65 V potential window, about 200 mV wider than that of SiWA which supports the hypothesis that replacing Si with B in the HPA can increase the electrochemical potential window due to the further negative potentials of the redox reactions. The open circuit potentials (OCPs) of the CNT-graphite electrodes in SiWA and BWA are also shown in Fig. 5. Each voltammogram was divided into two regions along the OCP. The amount of charge stored/delivered in region 1 was greater than that in region 2 in both CVs due to the reaction of the Keggin anions.

For any capacitor, during charging the potentials of both electrodes move against each other and away from the OCP, reaching their respective potential limit (E_{limit}). Tracking the state-of-charge and the actual potential of each electrode during charging and discharging reveals the reactions and allows deducing the mechanism within the electrochemical cells during operation. In this study, an external Ag/AgCl reference electrode was utilized as the 3rd electrode to monitor the potential of carbon electrodes in the supercapacitor cells.

Figs. 6a and b show the CV profiles of the SiWA- and BWA-based EDLCs as in Fig. 4a but with incremental cell voltages. E_{limit} of each electrode in the EDLC cell in Figs. 6a and b can be plotted as a function of the respective cell voltage (Figs. 6c and d). Also marked in Figs. 6c and d are the potential limits of the two HPAs obtained from Fig. 5 (-0.25 V and 1.2 V for SiWA; -0.45 V and 1.2 V for BWA). For an ideal symmetric supercapacitor, the change of potential for each electrode should be the same and the absolute slopes of the E_{limit} vs. cell voltage curves for the two electrodes should be identical. However, in both SiWA and BWA-based supercapacitors, due to the non-balanced charge capacity between region 1 and region 2 of the 3-electrode CV (Fig. 5), the absolute slopes of the E_{limit} vs. cell voltage curves for the two electrodes were different. The electrode that showed a faster increase with cell voltage (i.e. higher absolute slope) had a smaller capacity and vice versa.

In Figs. 6c and d, the E_{limit} of both positive electrodes showed a faster increase with cell voltage than that of the negative electrodes. This can be explained by the higher charge capacity at the negative electrodes due to the reaction of Keggin anions as seen in Fig. 5. It was easier for the negative electrode in the SiWA-based cell (Fig. 6c) to reach its anion

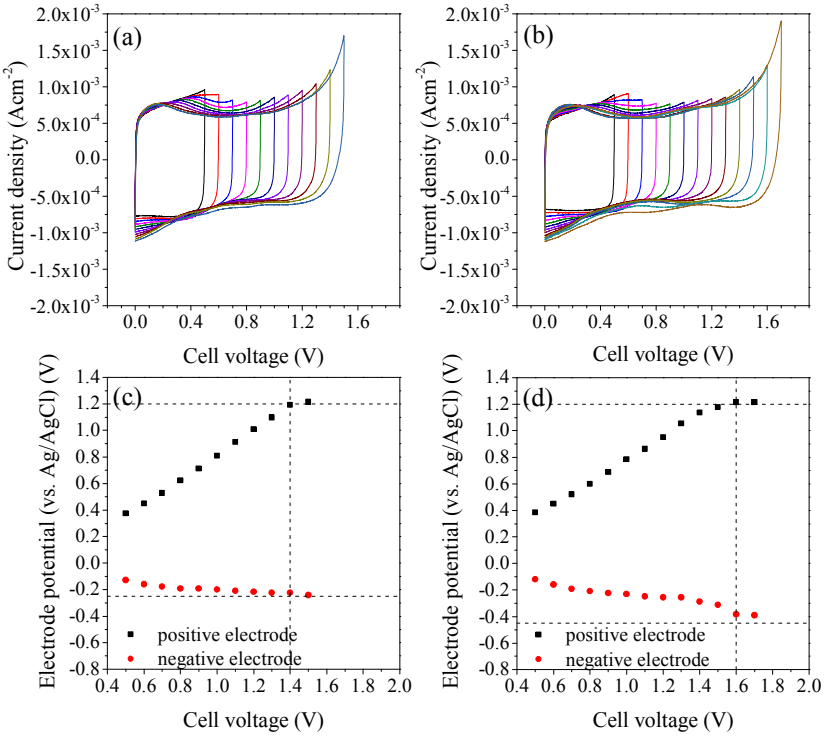

Figure 6: CVs of EDLC cells with 2 CNT-graphite electrodes in 0.05 M aqueous (a) SiWA from 0.5 V to 1.5 V; (b) BWA from 0.5V to 1.7 V; and the change in potential at the positive and negative electrodes of the capacitor during CV scan for 10th cycle as a function of time for (c) the SiWA-based cell and (d) BWA-based cell.

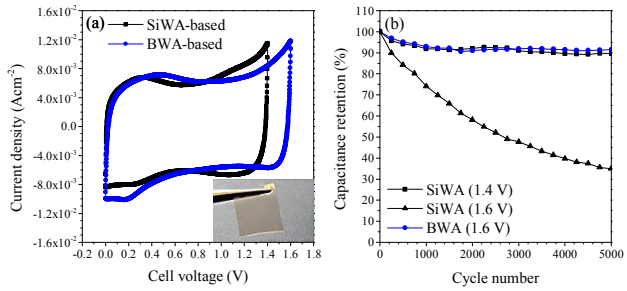

Figure 7: (a) CVs of two solid EDLCs with CNT-graphite electrodes using SiWA- and BWA-based polymer electrolytes at 1 Vs^{-1}. The inset shows a picture of a polymer electrolyte film; (b) Cycle life performance of the solid EDLCs using SiWA- and BWA-based polymer electrolytes at 1.4 V and 1.6 V cell voltages (current density = 1$mAcm^{-2}$).

reaction (at -0.25 V), leading to a further increase in the net charge at the negative electrode and causing an un-desirable increase in the slope of the E_{limit} curve of the positive electrode. As a result, the E_{limit} of the positive electrode in SiWA-based cell reached oxygen evolution at a cell voltage of 1.4 V. On the other hand, the BWA-enabled cell reached oxygen evolution at a cell voltage of 1.6 V because of a delayed anion reaction, explaining the higher maximum cell voltage of the BWA-based capacitor. Accordingly, to further enhance the voltage window, other HPAs with wider electrochemical stability windows can be developed.

BWA-based solid supercapacitors

The developed HPAs were incorporated in a PVA polymer host to form polymer electrolytes. Two types of solid CNT-graphite EDLCs with BWA-based and SiWA-based polymer electrolytes were constructed. Fig. 7a shows the CV overlays of the two solid cells cycled to their respective maximum cell voltage. Both capacitors achieved a near-rectangular-shaped profile at a scan rate of 1 Vs^{-1}, suggesting highly capacitive behavior at this high rate. The capacitance of the EDLCs was ca. 7 $mFcm^{-2}$, similar to the capacitance of the liquid EDLCs (Figs. 4a, 6a, and b). This indicates an intimate contact at the electrode/polymer electrolyte interface and good access to ions in the polymer electrolytes.

The other criterion of a good electrolyte for supercapacitors is its long-term stability and cycle life. The performance of constant-current cycling of the solid EDLCs is illustrated in Fig. 7b. The BWA-based device showed very stable performance with no significant decay in capacitance after being cycled for 5000 cycles between 0-1.6 V. In contrast, the capacitance of the SiWA-enabled device dropped by ca. 70% when cycled to 1.6 V. These results not only demonstrated the viability these HPA polymer electrolytes, but also confirmed the difference in voltage operating window of the two electrolytes. Further optimizations and characterizations of the BWA-based polymer electrolyte are under investigation.

Conclusions

$H_5BW_{12}O_{40}$ (BWA) was synthesized and characterized as proton conducting electrolyte for applications in liquid- and solid-state supercapacitors. The electrochemical performance of BWA was compared to $H_4SiW_{12}O_{40}$ (SiWA) and H_2SO_4 electrolytes as benchmark. BWA exhibited higher ionic conductivity than SiWA and H_2SO_4 at the same concentrations and achieved a potential window comparable to H_2SO_4, ca. 200 mV wider than that of SiWA. Both BWA-based solid and liquid EDLCs showed good capacitive response at high rates and exhibited a maximum cell voltage of 1.6 V. BWA proved to be a promising electrolyte for solid-state supercapacitors.

Through in-situ electrode potential tracking, an increased negative potential for the anion reaction in BWA was unveiled which led to a wider electrochemical stability window than for SiWA-based capacitors. Understanding the fundamentals of the interaction between electrolyte and electrode materials in a cell allowed us to select a proper chemistry and suitable device components and match them to design high-energy and high-power supercapacitors.

Acknowledgements

We appreciate the financial support from NSERC Canada. H. Gao would like to acknowledge an NSERC Alexander Graham Bell Canada Graduate Scholarship and a Hatch Graduate Scholarships for Sustainable Energy Research.

References

1. H. Gao and K. Lian, *RSC Adv.*, 2014, **4**, 33091-33113.
2. M. Maréchal, J. L. Souquet, J. Guindet and J. Y. Sanchez, *Electrochem. Commun.*, 2007, **9**, 1023-1028.
3. S. Slade, S. Campbell and T. Ralph, *J. Electrochem. Soc.*, 2002, **149**, A1556-A1564.
4. J. Sumner, S. Creager, J. Ma and D. DesMarteau, *J. Electrochem. Soc.*, 1998, **145**, 107-110.
5. Y. Xie, Y. Liu, Y. Zhao, Y. H. Tsang, S. P. Lau, H. Huang and Y. Chai, *J. Mater. Chem. A*, 2014, **2**, 9142-9149.
6. Q. Chen, X. Li, X. Zang, Y. Cao, Y. He, P. Li, K. Wang, J. Wei, D. Wu and H. Zhu, *RSC Adv.*, 2014, **4**, 36253-36256.
7. C. Yang, J. Shen, C. Wang, H. Fei, H. Bao and G. Wang, *J. Mater. Chem. A*, 2014, **2**, 1458-1464.
8. H. Gao and K. Lian, *J. Mater. Chem.*, 2012, **22**, 21272.
9. M. Kourasi, R. G. A. Wills, A. A. Shah and F. C. Walsh, *Electrochim. Acta*, 2014, **127**, 454-466.
10. A. Hardwick, P. G. Dickens and R. C. T. Slade, *Solid State Ionics*, 1984, **13**, 345-350.
11. K. D. Kreuer, M. Hampele, K. Dolde and A. Rabenau, *Solid State Ionics*, 1988, **28–30, Part 1**, 589-593.
12. R. C. T. Slade, H. A. Pressman and E. Skou, *Solid State Ionics*, 1990, **38**, 207-211.
13. R. C. T. Slade, J. Barker and H. A. Pressman, *Solid State Ionics*, 1988, **28–30, Part 1**, 594-600.
14. U. B. Mioč, M. R. Todorović, M. Davidović, P. Colomban and I. Holclajtner-Antunović, *Solid State Ionics*, 2005, **176**, 3005-3017.
15. M. Sadakane and E. Steckhan, *Chem. Rev.*, 1998, **98**, 219-238.
16. D. E. Katsoulis, *Chem. Rev.*, 1998, **98**, 359-388.
17. K. Lian and C. Li, *Electrochem. Solid-State Lett.*, 2008, **11**, A158-A162.

18. K. Lian and C. M. Li, *Electrochem. Solid-State Lett.*, 2009, **12**, A10-A12.
19. N. Giordano, P. Staiti, A. S. Aricò, E. Passalacqua, L. Abate and S. Hocevar, *Electrochim. Acta*, 1997, **42**, 1645-1652.
20. N. Giordano, A. S. Aricò, S. Hocevar, P. Staiti, P. L. Antonucci and V. Antonucci, *Electrochim. Acta*, 1993, **38**, 1733-1741.
21. A. D. S. Gomes and J. C. Dutra Filho, *Int. J. Hydrogen Energy*, 2012, **37**, 6246-6252.
22. Y. Xiang, M. Yang, J. Zhang, F. Lan and S. Lu, *J. Membr. Sci.*, 2011, **368**, 241-245.
23. M. Amirinejad, S. S. Madaeni, M. A. Navarra, E. Rafiee and B. Scrosati, *J. Power Sources*, 2011, **196**, 988-998.
24. J. J. Altenau, M. T. Pope, R. A. Prados and H. So, *Inorg. Chem.*, 1975, **14**, 417-421.
25. H. Gao and K. Lian, *J. Power Sources*, 2011, **196**, 8855-8857.
26. G. Fu, E. Wang, J. Liu and R. Zheng, *Acta Chim. Sinica*, 1985, **43**, 949-954.
27. H. Gao, A. Virya and K. Lian, *Electrochim. Acta*, 2014, **138**, 240-246.
28. Q. Tian and K. Lian, *Electrochem. Solid-State Lett.*, 2010, **13**, A4-A6.
29. H. Gao, Q. Tian and K. Lian, *Solid State Ionics*, 2010, **181**, 874-876.
30. C. Rocchiccioli-Deltcheff, R. Thouvenot and R. Franck, *Spectrochim. Acta, Part A*, 1976, **32**, 587-597.
31. U. Mioč, P. Colomban and A. Novak, *J. Mol. Struct.*, 1990, **218**, 123-128.
32. B. W. L. Southward, J. S. Vaughan and C. T. Oconnor, *J. Catal.*, 1995, **153**, 293-303.
33. C. Rocchiccioli-Deltcheff, M. Fournier, R. Franck and R. Thouvenot, *Inorg. Chem.*, 1983, **22**, 207-216.
34. C. W. Hu, M. Hashimoto, T. Okuhara and M. Misono, *J. Catal.*, 1993, **143**, 437-448.
35. D. H. Brown, *Spectrochim. Acta*, 1963, **19**, 585-587.
36. C. J. Gomez-Garcia, C. Gimenez-Saiz, S. Triki, E. Coronado, P. Le Magueres, L. Ouahab, L. Ducasse, C. Sourisseau and P. Delhaes, *Inorg. Chem.*, 1995, **34**, 4139-4151.
37. J. Wang, P. Ma, J. Li and J. Niu, *Chem. Res. Chinese U.*, 2007, **23**, 263-267.
38. O. Nakamura, I. Ogino and T. Kodama, *Solid State Ionics*, 1981, **3–4**, 347-351.
39. P. A. Jalil, M. A. Al-Daous, A. R. A. Al-Arfaj, A. M. Al-Amer, J. Beltramini and S. A. I. Barri, *Appl. Catal., A*, 2001, **207**, 159-171.
40. U. Mioč, R. Dimitrijević, M. Davidović, Z. Nedić, M. Mitrović and P. Colomban, *J. Mater. Sci.*, 1994, **29**, 3705-3718.
41. A. Horky, N. P. Kherani and G. Xu, *J. Electrochem. Soc.*, 2003, **150**, A1219-A1224.
42. P. Vanysek, in *CRC handbook of chemistry and physics*, ed. W. M. Haynes, CRC Press, 2013, vol. 5, pp. 77-79.
43. P. L. Taberna, P. Simon and J. F. Fauvarque *J. Electrochem. Soc.*, 2003, **150**, A292-A300.
44. S. Dong, X. Xi and M. Tian, *J. Electroanal. Chem.*, 1995, **385**, 227-233.
45. B. Keita and L. Nadjo, *J. Electroanal. Chem. Interfacial Electrochem.*, 1987, **217**, 287-304.

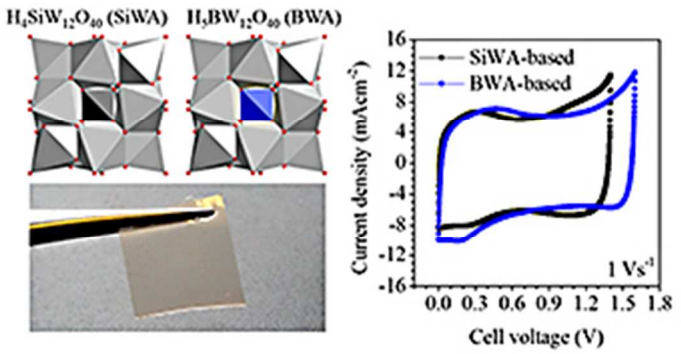

133x61mm (72 x 72 DPI)